



Acidity-targeting transition-aided universal chimeric antigen receptor T-cell (ATT-CAR-T) therapy for the treatment of solid tumors

Tianyu Shi ^{a,1}, Mengna Sun ^{a,1}, Subiyinuer Tuerhong ^{a,1}, Mengru Li ^a, Jiayu Wang ^a, Yingxin Wang ^a, Qinghua Zheng ^b, Lu Zou ^a, Changchang Lu ^d, Zhichen Sun ^c, Zhengyun Zou ^a, Jie Shao ^c, Juan Du ^c, Rutian Li ^{c,**}, Baorui Liu ^{c,***}, Fanyan Meng ^{a,b,*}

^a Department of Oncology, Nanjing Drum Tower Hospital Clinical College of Nanjing University of Chinese Medicine, Nanjing 210008, China

^b Department of Laboratory Medicine, Nanjing Drum Tower Hospital, The Affiliated Hospital of Medical School, Nanjing University, Nanjing 210008, China

^c Department of Oncology, Nanjing Drum Tower Hospital, The Affiliated Hospital of Medical School, Nanjing University, Nanjing 210008, China

^d Cancer Institute (Key Laboratory of Cancer Prevention and Intervention, China National Ministry of Education), The Second Affiliated Hospital, Zhejiang University School of Medicine, Hangzhou 310009, China

ARTICLE INFO

Keywords:

CAR-T cells

Tumor immunotherapy

pHLIP

Acidic tumor microenvironment

ATT-CAR-T

ABSTRACT

The use of CAR-T cells in treating solid tumors frequently faces significant challenges, mainly due to the heterogeneity of tumor antigens. This study assessed the efficacy of an acidity-targeting transition-aided universal chimeric antigen receptor T (ATT-CAR-T) cell strategy, which is facilitated by an acidity-targeted transition. Specifically, the EGFRvIII peptide was attached to the N-terminus of a pH-low insertion peptide. Triggered by the acidic conditions of the tumor microenvironment, this peptide alters its structure and selectively integrates into the membrane of solid tumor cells. The acidity-targeted transition component effectively relocated the EGFRvIII peptide across various tumor cell membranes; thus, allowing the direct destruction of these cells by EGFRvIII-specific CAR-T cells. This method was efficient even when endogenous antigens were absent. In vivo tests showed marked antigen modification within the acidic tumor microenvironment using this component. Integrating this component with CAR-T cell therapy showed high effectiveness in combating solid tumors. These results highlight the capability of ATT-CAR-T cell therapy to address the challenges presented by tumor heterogeneity and expand the utility of CAR-T cell therapy in the treatment of solid tumors.

1. Introduction

CAR-T-cell therapy has been actively developed and has demonstrated promising tumor regression in patients with hematological malignancies [1–3]. The development of novel strategies to increase the antitumor immune response and extend CAR-T-cell therapy to solid tumors is increasing [4,5]. The expression of tumor-specific antigens (TSAs) is pivotal for enabling the recognition of cells by CAR-T cells and inducing specific killing effects [6]. However, the utilization of CAR-T cell therapy in solid tumors is restricted by the shortage of specific antigens [7,8]. Genetic modification of T cells to express bispecific CAR or adjunct cytokines has been explored to target solid tumors.

Nevertheless, these strategies have still shown significant toxicity in patients. A primary factor is their inability to overcome the constraints posed by the absence of precise targets.

To comprehend the adaptive mechanisms of cancer cells and discover new strategies to effectively target solid tumor tissue, it is imperative to recognize the spatial and temporal complexity of the tumor microenvironment (TME) and its influence on tumor function. The TME constitutes a dynamic and heterogeneous system characterized by interactions between cellular and non-cellular components across various spatial and temporal scales. The acidic nature of the TME has garnered significant scientific attention in recent decades. The physicochemical composition of the TME differs from that of normal tissue,

* Corresponding author. Department of Oncology, Nanjing Drum Tower Hospital Clinical College of Nanjing University of Chinese Medicine, Nanjing 210008, China.

** Corresponding author.

*** Corresponding author.

E-mail addresses: rutianli@nju.edu.cn (R. Li), baoruiliu@nju.edu.cn (B. Liu), fanyanmeng@hotmail.com (F. Meng).

¹ These authors contributed equally: Tianyu Shi, Mengna Sun, Subiyinuer Tuerhong.

primarily due to deregulated energy metabolism, uncontrolled growth, and inadequate nutrient delivery [9]. Reduced nutrient delivery typically leads to decreased O₂ delivery and the accumulation of acidic metabolic byproducts.

Consequently, tumor pH values as low as 5.6 have been measured in human tumors, although most recorded values range from 6.4 to 7 [10]. Therefore, the acidic TME can be considered a crucial factor for tumor localization, and targeting acidity may offer advantages compared to current approaches. The pH Low Insertion Peptide (pHLIP) effectively senses and responds to the acidic environment typical of many solid tumors. Under acidic conditions, pHLIP undergoes a transition from a coil to a helix, allowing it to integrate into tumor cell membranes with the C-terminus positioned internally and the N-terminus externally. Consequently, pHLIP serves as an optimal agent for targeting the acidic tumor microenvironment (TME). pHLIP originates from the C-helix of bacteriorhodopsin [11] and exhibits a sequential pattern: an N-terminal flanking region rich in polar residues, a transmembrane domain predominantly hydrophobic yet containing pivotal residues that prevent insertion at physiological pH, and an optional C-terminal flanking region with additional pivotal residues [12]. Cargo molecules can attach to either terminus through a singular cysteine or lysine residue. The ability of pHLIP to self-assemble in tumor cells has been validated across various solid cancer types [13–15]. Thus, we propose that pHLIP could facilitate the targeting of diverse solid tumors by exogenous antigens.

The tumor microenvironment is characterized by mild acidity. Here, we propose a novel therapeutic approach for CAR-T cells, termed acidity-target transition aided universal chimeric antigen receptor T cell (ATT-CAR T), which uses the acidic conditions of the tumor microenvironment (TME). In our investigation, we focused on epidermal growth factor receptor variant III (EGFRvIII), a mutation resulting from the deletion of exons 2–7 in the EGFR gene, which hinders the receptor's binding to any known ligand [16]. EGFRvIII is specifically expressed on certain tumor cells but is absent in normal tissues, making it an ideal target for CAR-T cell therapy [17]. Consequently, we selected the EGFRvIII (EvIII) peptide as a neoantigen to attach to the N-terminus of pHLIP, resulting in pEvIII (Fig. S1a). This approach enables

EvIII-specific CAR-T cell activators to be displayed on tumor cell membranes within the mildly acidic tumor microenvironment, offering the potential for CAR-T cell-mediated immunotherapy of solid tumors (Fig. 1a and b). Moreover, EvIII-specific universal CAR-T cells have successfully targeted various solid tumors.

2. Methods

2.1. Synthesis of peptides

The pHLIP, EvIII, and pEvIII (ACEQNPIYWAR-YADWLFITPLLLLDLALLVDADEGTLEEKKGNYVVDH) were synthesized using ChinaPeptides Co., Ltd. The purity of all peptides was ~98 %.

2.2. Cell culture

The study employed human melanoma cells (A375), gastric mucosal epithelial cells (MKN45), triple-negative breast cancer cells (MDA-MB-231), murine breast cancer cells (4T1), and murine colon carcinoma cells (CT26). These cell lines were acquired from the Cell Bank of the Shanghai Institute of Biochemistry and Cell Biology. Specifically, MDA-MB-231 cells were genetically modified via retroviral transduction to facilitate the expression of firefly luciferase. A375, MKN45, 4T1, and CT26 cell lines were cultured in RPMI 1640 medium supplemented with 10 % fetal bovine serum (FBS), while MDA-MB-231 cells were cultured in DMEM-H medium (Gibco, USA), also supplemented with 10 % FBS. All cell cultures were maintained at 37 °C in an environment containing 5 % CO₂, with regular checks for mycoplasma contamination.

2.3. Cell membrane modification with pHLIP

A375 cells were seeded at a density of 5×10^5 cells per well in a 6-well plate, with 2 mL of medium adjusted to either pH 6.6 or pH 7.4. Various concentrations of pEvIII (0, 0.33, 1, 3, 9, 27, and 81 $\mu\text{g mL}^{-1}$) were added and then incubated with the cells for 4 h at 37 °C. After the

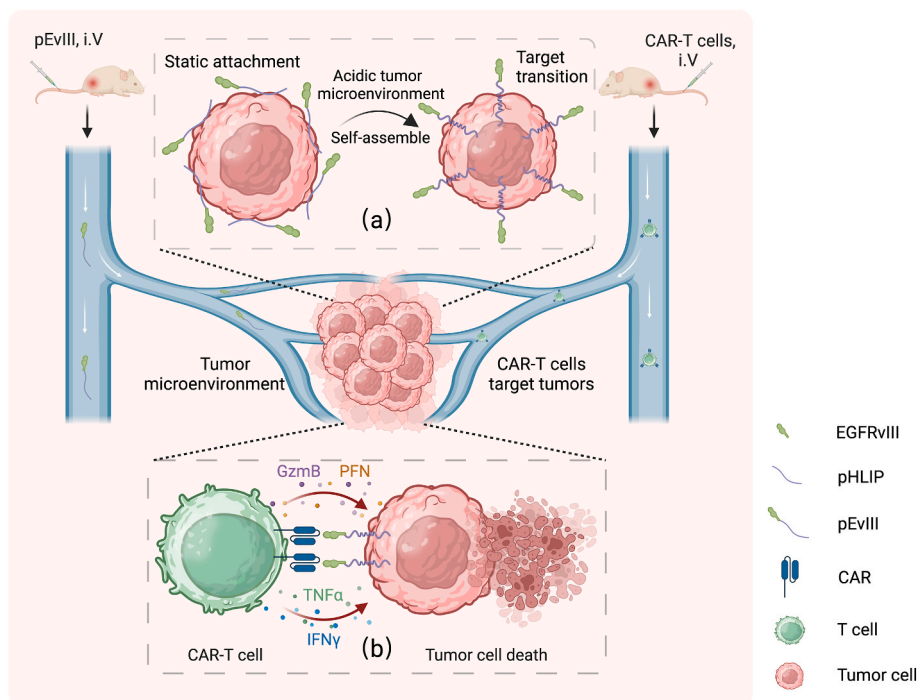


Fig. 1. The design of ATT-CAR-T cells and the immunotherapeutic mechanism involved. (a) pEvIII is injected intravenously into mice and circulates to the tumor site for self-assembly deformation and insertion into the tumor cell membrane, where it is exposed to the N-terminal antigen. (b) EGFRvIII antigens induce EGFRvIII-specific CAR-T-cell death.

incubation, the cells underwent three consecutive washes with PBS adjusted to pH 6.6 or 7.4. Subsequently, they were subjected to a 1-h incubation with a monoclonal antibody (mAb) against EGFRvIII (clone L8A4, Absolute Antibody), followed by a subsequent 1-h incubation with a PE-labeled anti-mouse IgG secondary antibody (BioLegend). Each incubation step was followed by three washes with PBS (pH 6.6 or 7.4). Cell collection and analysis were conducted using a BD Accuri C6 flow cytometer (BD Bioscience, USA) and analyzed with FlowJo software.

2.4. Confocal microscopy

Tumor cells were exposed to pEvIII at both pH 6.6 and 7.4 for a duration of 4 h at 37 °C. Following this incubation period, they underwent incubation with a monoclonal antibody against EGFRvIII and a PE-labeled anti-mouse IgG secondary antibody for 1 h. Each incubation step was succeeded by three washes with PBS (pH 6.6/pH 7.4). The nuclei were stained with DAPI (Beyotime, Shanghai, China) for 10 min at room temperature. Subsequently, the stained cells were carefully observed under a confocal laser scanning microscope (Leica, Germany), allowing for precise visualization of the distribution of pEvIII within the tumor cells.

2.5. Biodistribution and immunohistochemical staining

For biodistribution and in vivo imaging analysis, Cy5-labeled EvIII or pEvIII was synthesized to determine its systemic distribution and tumor-targeting capability. Briefly, 0.1 mg of Cy5 Mono NHS ester was reacted with 500 µL of EvIII or pEvIII in PBS (0.1 mg mL⁻¹), and the mixture was incubated at 4 °C for 12 h with gentle agitation in a 1.0 mL Eppendorf tube. After synthesis, PBS-Cy5, EvIII-Cy5, and pEvIII-Cy5 were intravenously injected into nude mice bearing MDA-MB-231 tumors. The biodistribution of the labeled peptides in the mice was tracked over time using an In Vivo Imaging System (IVIS) (PerkinElmer, Massachusetts, USA). After 48 h of injection, the mice were euthanized, and their organs, including the tumors, were extracted for imaging analysis. This analysis offered valuable insights into the systemic distribution and accumulation of the peptides within the tumors.

For immunohistochemical analysis, mice harboring subcutaneous MDA-MB-231 tumors were intravenously injected with Cy5, EvIII-Cy5, and pEvIII-Cy5 at a concentration of 0.2 mg mL⁻¹ (100 µL). The study aimed to evaluate the distribution of the peptides in organs and their potential to induce morphological changes. Vital organs such as the heart, liver, spleen, lung, and kidney were collected at specific intervals for Hematoxylin and Eosin (H&E) staining, allowing for the examination of any morphological alterations. Concurrently, excised tumors underwent immunostaining: cryosections were labeled with an anti-EGFRvIII antibody, PE-labeled anti-mouse IgG secondary antibody, and DAPI. These sections were then analyzed using a Leica confocal microscope (Germany), providing a detailed understanding of the peptides' ability to target tumors and interact with tumor cells.

2.6. Generation of EGFRvIII CAR-T cells

To produce the virus, retroviral supernatant was collected from 293T cells. This involved transfecting 2 µg of pMD2.G envelope plasmid, 6 µg of psPAX2 packaging plasmid, and 8 µg of EGFRvIII transfer plasmid into 293T cells cultured in 100 mm dishes at 80 % confluency. The transfection was carried out using PEI MW 40000 (Yeasen Biotechnology, Shanghai) for transient transfection. The media was replaced with fresh media after 6 h, and the media was replenished every 24 h. The retroviral supernatant was collected at 48 and 72 h post-transfection following the removal of cell debris. Subsequently, the supernatant was subjected to 200-fold enrichment using a virus concentration kit (Cat #C2901 M, Beyotime) before being stored at -80 °C.

For the generation of human CAR-T cells, primary T cells were isolated from peripheral blood mononuclear cells (PBMCs), obtained from

healthy volunteers at Nanjing Drum Tower Hospital, using the Ficoll density gradient centrifugation method. Informed consent was obtained from all donors for research purposes. On day 0, human T cells were cultured and stimulated with anti-human CD3 (4 µg mL⁻¹) and CD28 (8 µg mL⁻¹) antibodies (Biolegend, San Diego) in AIM-V medium (Thermo Fisher) supplemented with 10 % FBS, 300 IU mL⁻¹ IL-2, ten ng mL⁻¹ IL-7, and ten ng mL⁻¹ IL-15 (Sino, Beijing). On day 2, retrovirus supernatant (5 × 10⁸ TU mL⁻¹, 50 µL) mixed with 950 µL of medium composed of AIM-V medium supplemented with 0 % FBS, was added to 12-well plates (pre-coated the plates with RetroNectin (Takara)) at a volume of 1 mL per well, followed by centrifugation at 3200 RPM, 32 °C for 2 h. The supernatant was removed, and T cells (5 × 10⁵/well) were seeded in 12-well plates. The plates were gently centrifuged at 1200 RPM for 2 min and then incubated for 48 h. This transduction process was repeated on day 4, after which the cells were further expanded until day 10.

For mouse CAR-T-cell generation, splenocytes were obtained from 6-week-old female BALB/c mice following the established in vitro stimulation protocol for mouse T cells [18]. Briefly, the spleen was processed into single-cell suspensions, and CD3⁺ T cells were isolated using the MojoSort Mouse CD3 T-Cell Isolation Kit (Cat #480021, Biolegend) per the supplier's guidelines. On day 0, the isolated T cells were cultured and stimulated with anti-mouse CD3/CD28 antibodies (5 µg mL⁻¹, Bio X cell) in RPMI 1640 medium supplemented with 10 % FBS and 500 IU mL⁻¹ IL-2. On day 2, mouse T cells were infected with recombinant lentiviruses at an MOI of 20–50. The centrifugation step was repeated, and the cells were cultured for 3–4 days for expansion.

2.7. Cytotoxicity studies and T-cell activation

In the cytotoxicity investigation, T/CAR-T cells functioned as effector cells, while MDA-MB-231, MKN45, and A375 tumor cells served as target cells. We seeded 2 × 10⁴ MDA-MB-231 or A375 tumor cells into a 96-well plate and treated them with 0.1 mL of pEvIII (9 µg mL⁻¹) at pH 6.8 or 7.4 for 4 h, followed by coculture with CAR-T cells at an effector-to-target cell ratio of 10:1 for an additional 5–6 h. Similarly, we seeded 2 × 10⁴ MKN45 cells into a 96-well plate and treated them with 0.1 mL of pEvIII (concentrations of 0, 0.33, 1, 3, 9, or 27 µg mL⁻¹) at pH 6.6 or 7.4 for 4 h before coculturing with T/CAR-T cells at the same effector-to-target cell ratio for another 5–6 h. Cytotoxicity was evaluated using the CFSE/PI labeling cytotoxicity assay.

$$\text{Cytotoxicity\%} = \frac{\text{CFSE}^+ \text{PI}^+}{\text{CFSE}^+}$$

For the investigation of T-cell activation, 2 × 10⁴ MDA-MB-231 tumor cells were seeded in a 96-well plate. These cells were then treated with 0.1 mL of pEvIII (9 µg mL⁻¹) at pH 6.8 or 7.4 for 4 h, followed by coculture with CAR-T cells at an effector-to-target ratio of 20:1 for an additional 24 h. T-cell activation was assessed using flow cytometry with anti-human CD69-APC staining. Subsequently, the supernatants were collected to measure cytokine release using the Human Th1/Th2 Cytokine Kit (BD Biosciences, NZ, USA).

2.8. Therapeutic studies in vivo

All experiments involving mice were obtained from Shanghai Sippr-BK Laboratory Animal Co. Ltd. (Shanghai, China) and conducted at the Laboratory Animal Center of the Affiliated Nanjing Drum Tower Hospital of Nanjing University Medical School. The Ethics Committee of Nanjing Drum Tower Hospital approved all experiments in this study (ethics approval number/ID: 20230611). In a human breast cancer tumor model, MDA-MB-231-luc cells (1.0 × 10⁷) were implanted into the mammary fat pad of each BALB/c nude mouse (female, five weeks old, weighing 13–15 g). Treatment commenced when tumor volumes reached approximately 50 mm³. Mice received intravenous administrations of 100 µL PBS, pEvIII (0.1 mg mL⁻¹, 100 µL), CAR-T cells (100 µL, 1 × 10⁷), or a combination of pEvIII + CAR-T cells. In the pEvIII +

CAR-T cell group, CAR-T cells were administered 12 h after pEvIII treatment. All treatments were given over five days with a total of two injections. Tumor volume and body weight were monitored daily. Tumor dimensions were measured using a digital caliper, and tumor volume was calculated using the formula $\text{width}^2 \times \text{length} / 2$. The animals were humanely euthanized when the tumor volume exceeded 1500 mm³.

For the immunocompetent mouse model, female BALB/c mice (6 weeks old, weighing 18–25 g) were subcutaneously inoculated with 2×10^6 CT26 cells or 4T1 cells. Treatment began when the tumor volume reached approximately 50 mm³, following the previously established treatment cycle. On day 26, all BALB/c mice were euthanized, and their tumor tissues were collected. The tissues underwent digestion with collagenase type IV (1 mg mL⁻¹, Sigma) at 37 °C for 2 h, followed by mechanical disaggregation to achieve a single-cell suspension. To quantify dendritic cells (DCs) within the tumors, we used a PE-conjugated anti-CD11c monoclonal antibody, an APC-conjugated anti-mouse CD80 monoclonal antibody, and a PC7-conjugated anti-mouse CD86 monoclonal antibody to evaluate the number and activation status of the DCs. All monoclonal antibodies were procured from Biolegend.

2.9. Biosafety evaluations

To examine the immune response to systemic inflammation triggered by EvIII-CAR-T cells, mice with tumors were given ATT CAR-T cells intravenously. After 48 h, levels of IFN- γ , IL-2, IL-13, IL-5, IL-6, and TNF- α were assessed using the MU Th1/Th2 Panel (Cat #C2901 M, Biolegend), alongside measuring biochemical markers (BUN, CREA, ALT, AST, ALP). Following the experiment's conclusion, all mice were euthanized, and their organs—heart, liver, spleen, lungs, and kidneys—were gathered for hematoxylin-eosin (H&E) staining. Subsequent analyses were carried out using optical microscopy (DM5000, Leica, Germany).

2.10. Statistical analysis

All statistical analyses were performed using GraphPad Prism 8 software (*P < 0.05, **P < 0.01, and ***P < 0.001). Data were expressed as mean \pm SD or mean \pm SEM. Flow cytometry data were obtained with a BD Accuri C6 (BD Biosciences, USA) and processed using FlowJo software. All images were created using Affinity Designer.

3. Results

3.1. In vitro assessment of cell membrane antigen modification by pEvIII

Our investigation aimed to conjugate the EGFRvIII (EvIII) antigen to tumor cell membranes across various solid tumor types utilizing pH low insertion peptide (pHLIP) technology. A fully synthetic approach facilitated the integration of the EvIII antigen at the N-terminus of pHLIP, ensuring extracellular antigen display (Supplementary Fig. S1). Mass spectrometry (MS) verified the successful synthesis of the pEvIII fusion peptide (Supplementary Fig. S1), underscoring the necessity of verifying the presence of the antigen on the fusion construct without impairing the operational integrity of the pHLIP. We further explored the potential impact of fusion on the ability of pHLIP to modify tumor cell membranes. A concentration-dependent kinetics analysis was performed to determine the optimal conditions for cell membrane modification. A375 cells, at a density of 5×10^5 cells per well, were exposed to varying pEvIII concentrations at pH 6.6 for 4 h, followed by incubation with a PE-labeled anti-EGFRvIII antibody. Flow cytometry revealed a notable increase in cell modification efficiency, with over 95 % of cells exhibiting PE positivity at a pEvIII concentration of 9 $\mu\text{g mL}^{-1}$ (Fig. 2a). A further increase in concentration did not significantly augment this efficiency. Similar observations were recorded in MDA-MB-231 and MKN45 cells treated with pEvIII, with 9 $\mu\text{g mL}^{-1}$ established as the

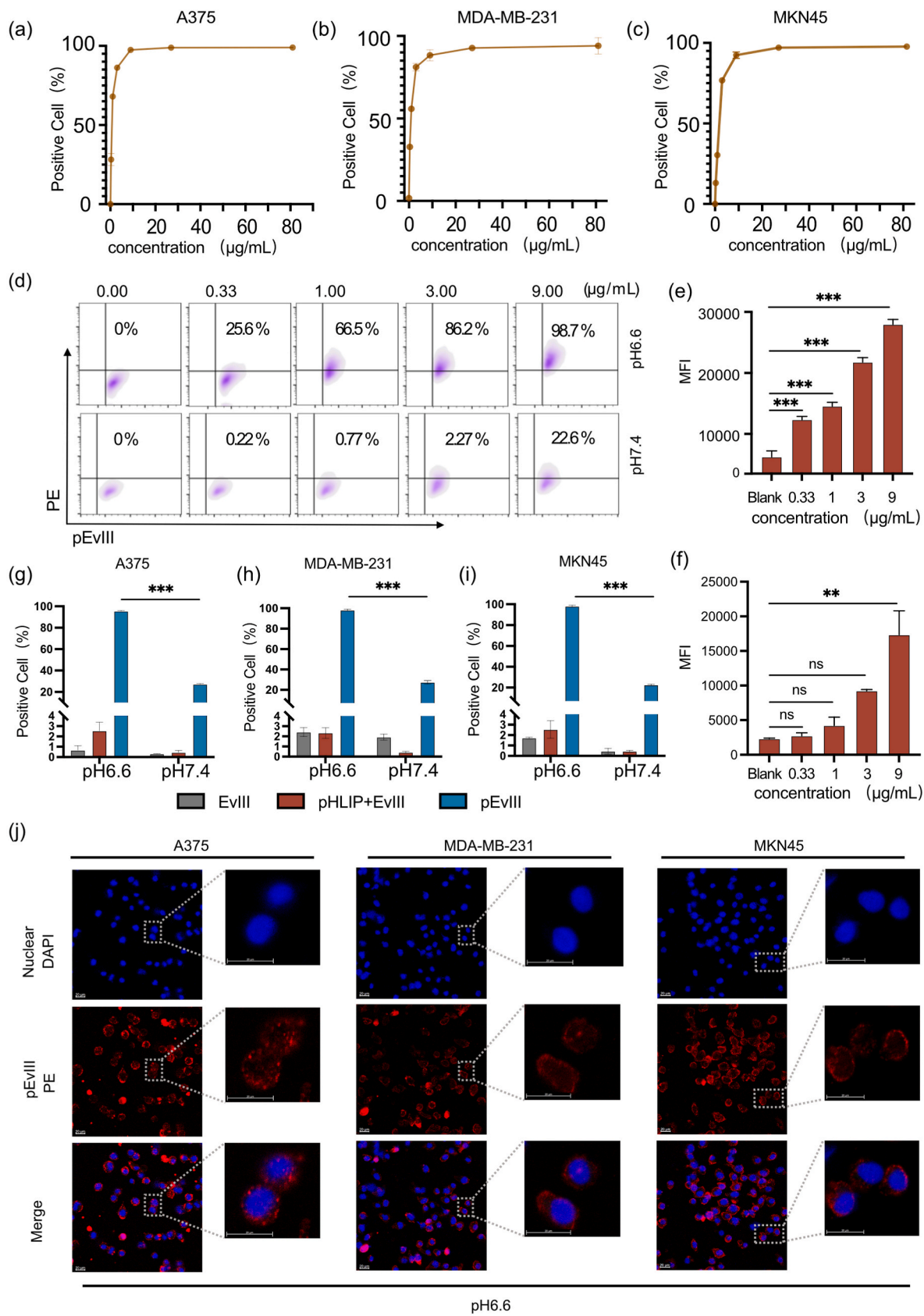
optimal concentration for membrane modification (Fig. 2b and c).

To evaluate the specificity of pEvIII membrane modification in response to environmental pH, we extended the study to a neutral pH of 7.4. Remarkably, at the optimal concentration of 9 $\mu\text{g mL}^{-1}$, the proportion of positive cells at pH 6.6 was fourfold greater than that at pH 7.4 (Fig. 2d–f, Supplementary Fig. S2), illustrating the pH-selective nature of pEvIII-mediated cell membrane modification. Comparative analysis with control groups (EvIII or pHLIP + EvIII) revealed that pEvIII-modified A375 cell membranes were more efficient, irrespective of pH, with a significantly greater modification rate observed at pH 6.6 than at pH 7.4 (Fig. 2g). This trend was consistent across other tumor cell lines (MKN45 and MDA-MB-231) when assessed against EvIII, pHLIP + EvIII, or pEvIII (Fig. 2h and i), indicating a pH-dependent mechanism of pHLIP-mediated antigen insertion. Confocal microscopy provided further evidence of the efficacy of pEvIII, showing pronounced PE fluorescence in tumor cells treated with pEvIII at pH 6.6 (Fig. 2j). Conversely, minimal fluorescence was detected after treatment at pH 7.4 (Supplementary Fig. S3), underscoring the pH-dependent precision of pEvIII in targeting tumor cell membranes for antigen loading. These findings collectively affirm the ability of pEvIII to facilitate antigen incorporation into tumor cell membranes under acidic conditions, revealing significant advancements in antigen presentation technology with potential implications for enhancing immunotherapeutic strategies against solid tumors.

3.2. In vivo metabolism and biodistribution of pEvIII

To elucidate the tumor-targeting capabilities and operational dynamics of pEvIII molecules within a mildly acidic in vivo microenvironment, we established a breast cancer model using MDA-MB-231 cells in BALB/c nude mice. This model allowed for a comparative assessment of the metabolism and distribution of fluorescently tagged EvIII (EvIII-Cy5) and pEvIII (pEvIII-Cy5), employing Cy5 for in vivo tracing. Intradermal injections of these fluorescent markers facilitated fluorescence measurement at 30-min intervals, up to 48 h post-administration (Fig. 3a). Whole-body imaging analyses revealed significant fluorescence enrichment in tumors at the 4-h mark, with pEvIII-Cy5 exhibiting notably enhanced tumor-targeting efficiency compared to EvIII-Cy5 (Fig. 3a). At the 48-h mark post-systemic administration, tumors and organs were harvested for analysis. Tumors from the pEvIII-Cy5 group displayed prolonged fluorescence (Fig. 3b and c). While fluorescence accumulation was noted in the liver and kidneys, these observations allowed for dynamic tracing of pEvIII alterations in these organs. Time-point analyses at 12, 24, and 48 h post-injection indicated initial peptide accumulation in the liver, attributed to its role in drug metabolism (Fig. 3d). However, as anticipated, the relative peptide concentration in the liver decreased over time, with a growing preference for tumor localization.

Immunohistochemical (IHC) analysis further supported the increased accumulation of pEvIII in tumor tissues, attributed to the pHLIP sequence (Fig. 3e). While faint fluorescence was observed in the liver and kidneys, IHC staining confirmed the absence of active antigen infiltration in major organs, such as the heart, liver, spleen, lungs, and kidneys. These results suggest inactive antigens or dyes without specific targeting functionality. Moreover, Hematoxylin and Eosin (H&E) staining validated the lack of organ damage following systemic delivery of pEvIII (Fig. 3f). Together, these findings emphasize the effectiveness of pHLIP in facilitating targeted antigen accumulation within tumor tissues while ensuring excellent biosafety profiles in vivo. The implications of these findings for enhancing CAR-T cell therapy and their potential translational significance in clinical settings are noteworthy, highlighting the feasibility of pEvIII as a promising approach for tumor-specific targeting and treatment.



(caption on next page)

Fig. 2. pEvIII-mediated cell membrane target transfer. (a, b, c) Flow cytometric analysis of A375, MDA-MB-231, and MKN-45 tumor cells exposed to pEvIII for varying durations at pH 6.6, and stained with anti-EGFRvIII antibody, PE-labeled anti-mouse IgG secondary antibody to assess cell-surface pEvIII ($n = 3$ independent experiments). (d) Representative flow cytometry plots illustrating the insertion efficiency of pEvIII at pH 6.6 or pH 7.4 ($n = 3$ independent experiments). (e) Mean fluorescence intensity (MFI), release of fluorescently labeled IgG from anti-EGFRvIII bound to A375 cells incubated with pEvIII at pH 6.6 (e) or pH 7.4 (f). (g–i) Effect of pEvIII-mediated target transfer on A375 tumor cells (g), MKN-45 tumor cells (h), MDA-MB-231 tumor cells (i), at pH 6.6 ($n = 3$ independent experiments). Data are presented as the mean \pm s.e.m. *** $p < 0.001$. Student's t-test was employed for statistical analysis (g, h, i). (j) Representative confocal microscopy images of tumor cells post pEvIII-mediated target transfer. A375 and MKN45 tumor cells were treated with pEvIII at pH 6.6 for specified durations, stained with PE and DAPI for analysis of cell-surface pEvIII. Staining: Tumor cells were exposed to recombinant mouse anti-EGFRvIII for 1 h; subsequently, they were incubated with PE-labeled anti-mouse IgG antibody for 1 h. Nuclei were stained with DAPI (Beyotime, Shanghai, China) for 10 min at room temperature. (Red: PE, blue: DAPI. Scale bar: 20 μ m). (For interpretation of the references to colour in this figure legend, the reader is referred to the Web version of this article.)

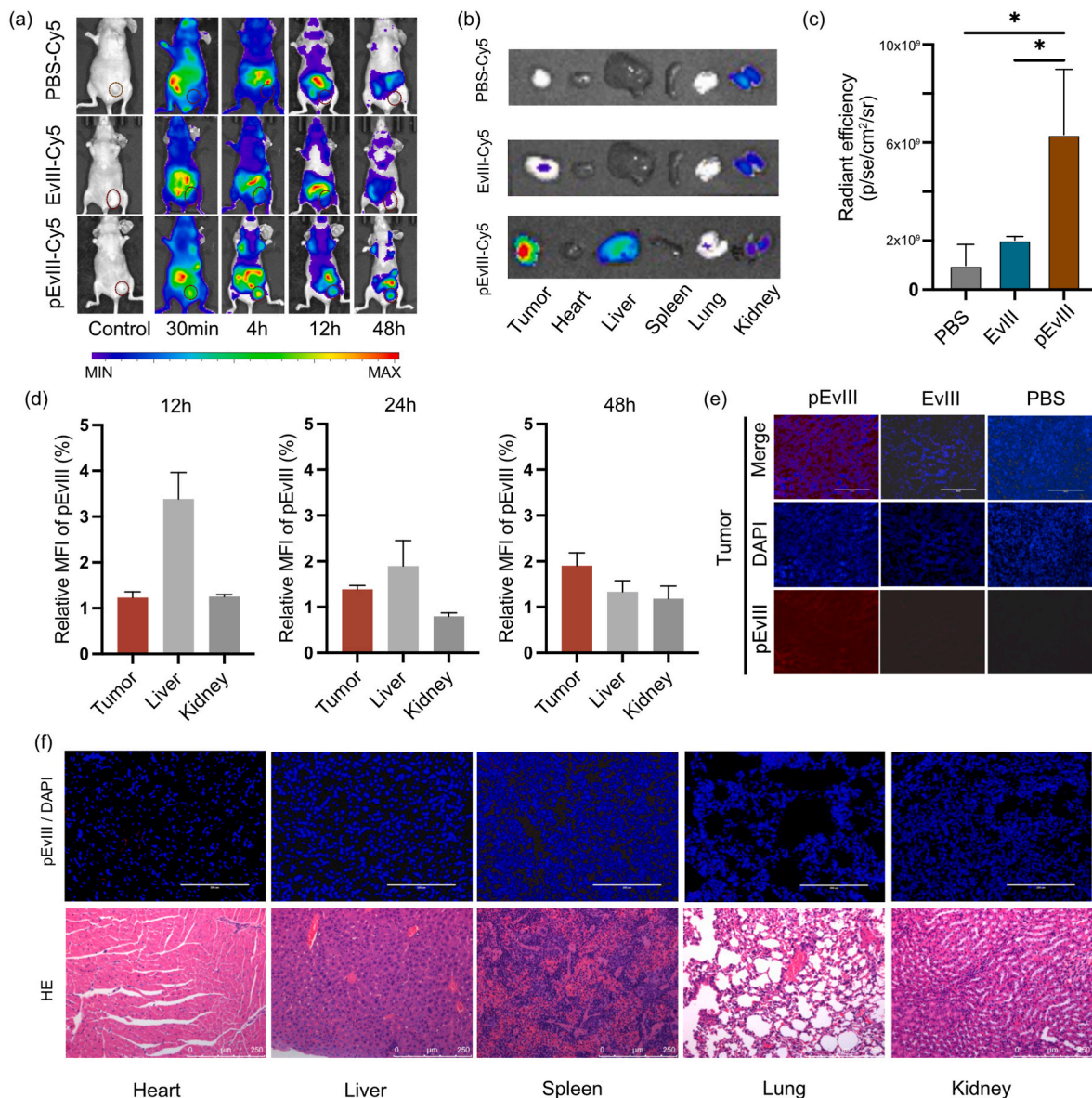


Fig. 3. Biodistribution and tumor target of pEvIII in vivo. (a) The in vivo imaging of EvIII-Cy5 and pEvIII-Cy5. (b, c) Biodistribution of EvIII-Cy5 and pEvIII-Cy5 in tumors and organs. Data are represented as the mean \pm s.e.m. * $P < 0.05$. Student's t-test was used for statistical analysis ($n = 3$ independent experiments). (d) Modification efficiency changes of pEvIII in tumor, liver, and kidney at different time points. The tissue was extracted and prepared into single-cell suspension, and the fluorescence intensity of the cy5 signal was detected by flow cytometry. (e) Immunofluorescence analysis of tumor after the treatment 48 h (Scale bar: 200 μ m). (f) After the treatment, immunofluorescence analysis (Scale bar: 200 μ m) and H&E staining of the major organs (Scale bar: 250 μ m).

3.3. In vitro immune response of EvIII-specific CAR-T cells

To assess the effectiveness of pEvIII-modified antigens in stimulating CAR-T cell-mediated cytotoxicity in vitro, we conducted experiments using EGFRvIII-specific CAR-T cells, which underwent 10 days of

transduction and expansion (Fig. 4a; Supplementary Fig. S5). We aimed to explore how adjusting the concentration of pEvIII could influence the cytotoxic ability of CAR-T cells and measured this relationship through tumor-killing kinetics (Fig. 4b and c). Coculturing EGFRvIII-specific CAR-T cells with tumor cells pre-treated with pEvIII for 24 h revealed

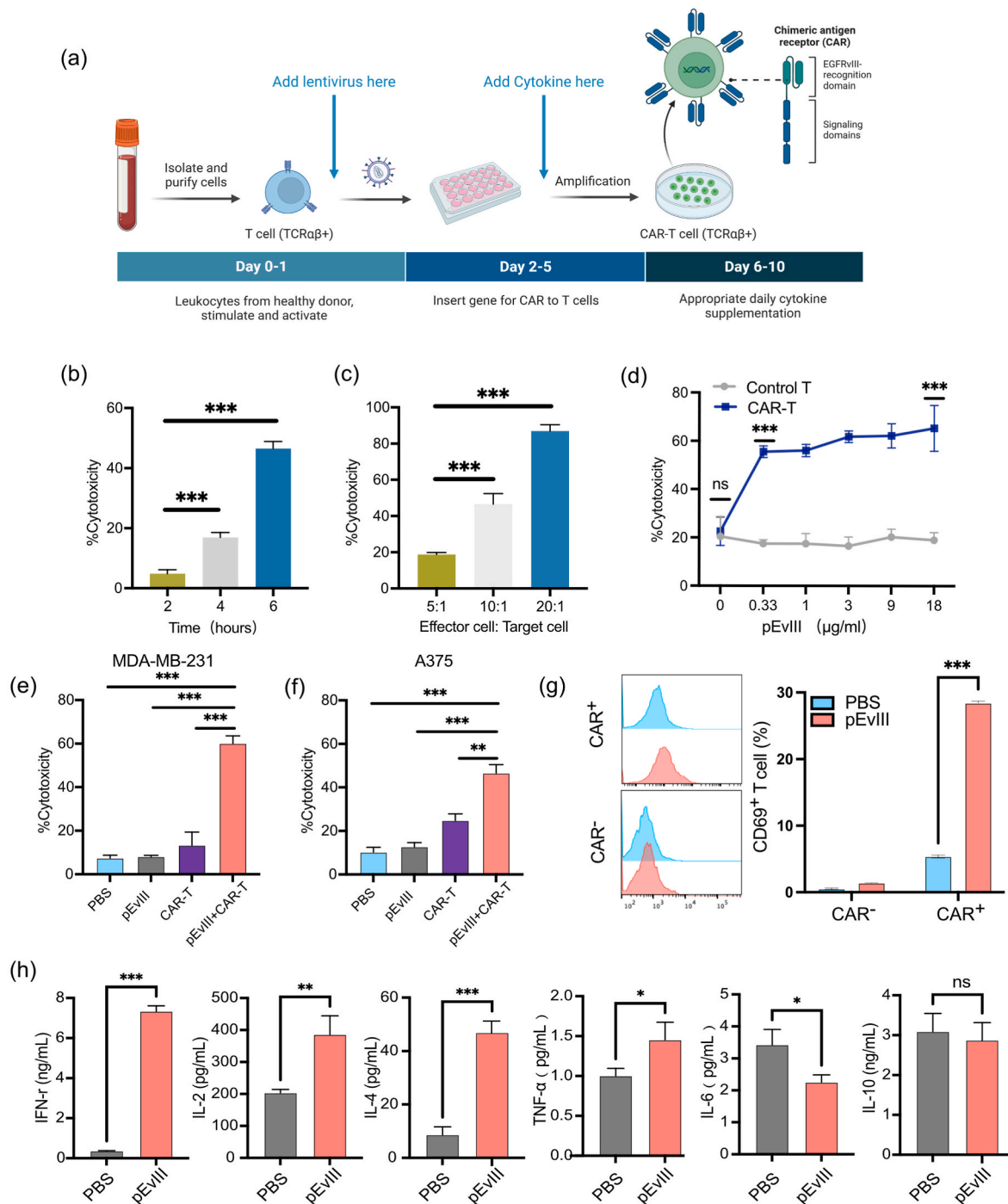


Fig. 4. In vitro pEvIII-mediated immune response of EvIII CAR-T cells (a) T cells were isolated from peripheral blood of volunteers, sorted, and transduced into CAR-T cells via lentivirus. (b,c) Kinetics of tumor-killing activity of EvIII-CAR-T cells. (d) Cytotoxicity of EvIII CAR-T cells and mock T cells against tumor cells treated with varying concentrations of pEvIII ($n = 3$), at an effector-to-target cell ratio of 10:1. (e, f) pEvIII-induced cytotoxic effects on MDA-MB-231 triple negative breast cancer cells and A375 melanoma cells ($n = 3$). (g) Expression of CD69 on CAR-negative and positive subpopulations after 24 h incubation with pEvIII-treated tumor cells ($n = 3$). (h) Cytokine production by EvIII CAR-T cells after coculture with MDA-MB-231 cells treated with indicated formulations ($n = 3$). Data presented as mean \pm s.e.m. * $P < 0.05$, ** $P < 0.01$, *** $P < 0.001$. Student's t-test used for statistical analysis (b, c, d, e, f, g, h).

a significant difference in cytotoxic activity. Mock-transfected T cells (mock T) exhibited minimal tumor cell lysis even at pEvIII concentrations up to 30 times the baseline (Fig. 4d). In contrast, CAR-T cells showed a threefold increase in tumor-killing efficiency compared to mock T cells (Fig. 4d). Notably, further increases in pEvIII concentration did not result in enhanced cytotoxicity, suggesting an optimal level of antigen modification for CAR-T cell activation. Combining pEvIII pretreatment with CAR-T cell therapy significantly boosted cytotoxicity

($59.8 \pm 3.5\%$) against MDA-MB-231 cells (Fig. 4e), surpassing the efficacy seen with CAR-T cell treatment alone. Conversely, control groups receiving PBS and pEvIII without CAR-T cells exhibited minimal tumor cell lysis. Similar results were observed in A375 melanoma cells, where the combination of pEvIII and CAR-T cells achieved a tumor-killing rate of $46.4 \pm 3.9\%$ (Fig. 4f).

The efficacy of CAR-T cell engagement and subsequent cytotoxicity relies on the coordinated activation of T cells and the directed release of

cytotoxic granules, leading to the demise of target cells [19]. IFN- γ , generated by antigen-stimulated CAR-T cells, has been shown to induce tumor cell death [20]. Our analyses revealed a significant increase in the production of IFN- γ by antigen-stimulated CAR-T cells, a key mediator of tumor cell demise, in the pEvIII + CAR-T treatment group (Supplementary Fig. S7). Evaluation of T cell activation markers demonstrated a significant upregulation of CD69, an early activation marker, in the CAR-positive subpopulation, with no notable changes in the CAR-negative group, further confirming the targeted stimulation of CAR-T cells by the modified antigens (Fig. 4g). Furthermore, the secretion profile of multiple cytokines indicated a robust Th1-type response in pEvIII CAR-T cell-mediated interactions, characterized by elevated levels of IFN- γ , TNF- α , and IL-2 compared to controls, indicating a potent inhibitory effect on tumor proliferation (Fig. 4h). Additionally, the rise in IL-4 levels, a cytokine known to impede tumor growth in correlation with IL-4R expression, underscores the multifaceted nature of CAR-T cell responses [21,22]. Cytokines associated with a Th2-type response, such as IL-10, remained unchanged. Taken together, these findings highlight the innovative potential of the ATT-CAR-T strategy in enabling the precise targeting of antigen-negative tumor cells within an acidic microenvironment. This approach represents a promising avenue for extending the utility of CAR-T cell therapies in addressing antigen-negative solid tumors, offering a new frontier in cancer immunotherapy.

3.4. In vivo therapeutic efficacy of CAR-T cells for solid tumors

To assess the effectiveness of pEvIII-targeted CAR-T cells against tumors in vivo, we first developed MDA-MB-231 breast cancer models. Tumor-bearing mice were randomly assigned to four treatment groups: PBS, pEvIII, CAR-T, and pEvIII + CAR-T (ATT-CAR-T). We noted that within the mildly acidic microenvironment, pEvIII binds to tumor tissue 4 h after intravenous injection (Fig. 3a). Notably, total body fluorescence decreased at 12 h post-injection, maintaining pronounced tumor visibility (Supplementary Fig. S4); consequently, CAR-T-cell administration was postponed for 12 h, and the treatments were administered biweekly for a total of two sessions [23] (Fig. 5a). Tumor progression was monitored through tumor volume measurement and bioluminescence imaging (Fig. 5b–f). Notably, the combination of CAR-T cells and pEvIII treatment yielded superior inhibition of tumor growth, achieving approximately 40 % of the tumor volume observed in the PBS control group (Fig. 5b). By day 21, markedly reduced luminescence signals were evident in the pEvIII + CAR-T group, indicating significant tumor suppression within the ATT-CAR-T treatment cohort (Fig. 5e and f). As depicted in Fig. 5c, this dual treatment approach markedly curtailed tumor growth and improved survival rates. Conversely, mice from all other treatment groups succumbed within 38 days. Furthermore, no significant fluctuations in body weight were observed throughout the treatment period (Fig. 5g).

Exploratory investigations extended to immunocompetent mouse models employing CT26 colon carcinoma and 4T1 breast cancer cells in BALB/c mice. Treatments with pEvIII and murine EGFRvIII-CAR-T cells were administered intravenously, with a regimen of two doses every five days. This approach significantly suppressed tumor growth in both cancer models, confirming the efficacy of the ATT-CAR-T-cell strategy across different tumor types (approximately 47 % for CT26 colon carcinoma and 67 % for 4T1 breast cancer) (Fig. 6a–c, Supplementary Fig. S9). There was no significant change in body weight during treatment (Supplementary Figs. S9 and S11). Despite the low rates of CAR-T-cell homing to tumor sites—likely a reflection of the immunosuppressive tumor microenvironment and inherent T-cell exhaustion—the treatment regimen noticeably increased the number of activated dendritic cells (DCs) within tumor locations (Figs. Fig. 6d–e and g). This observation aligns with the literature highlighting the pivotal role of DC activation in the aftermath of antigen release from apoptotic tumor cells [24,25], suggesting an indirect mechanism by which ATT-CAR-T cells facilitate

tumor cell eradication.

Our thorough analysis demonstrates that pEvIII-mediated antigen targeting enhances CAR-T cell cytotoxicity against solid tumors, representing a significant advancement in broadening the clinical utility of CAR-T therapy in cancer treatment. The identification of activated DCs at tumor sites following treatment offers an intriguing insight into the intricate interplay among targeted antigen delivery, CAR-T cell activation, and the endogenous immune response, paving the way for promising avenues in future research and therapeutic innovation in the field of cancer immunotherapy.

3.5. Biosafety profiles

In our final investigation phase, we meticulously examined the biosafety profile of Acidity-Targeted Transition-aided CAR-T (ATT-CAR-T) therapy to assess its impact on organ functionality—a crucial aspect for clinical application of cellular therapies. This assessment involved analyzing serum biochemical markers in treated mice, revealing no notable deviations from the baseline established by the PBS control group (Fig. 6f). Additionally, evaluation of serum concentrations for a panel of six inflammatory factors and chemokines—IL-2, IL-5, IL-6, IL-13, TNF- α , and IFN- γ —showed consistency across all treatment groups in Balb/c mice, indicating the absence of systemic inflammatory response or chemokine dysregulation attributable to ATT-CAR-T treatment (Fig. 6h). Although a significant reduction in some cytokines was observed in the pEvIII + CAR-T group, we attribute this to the activation mechanism of CAR-T cells and their antitumor effect [26–28].

Major organs such as the heart, liver, spleen, lungs, and kidneys were meticulously collected for histopathological examination to further assess biosafety. Hematoxylin and Eosin (H&E) staining of these organ tissues revealed no histological abnormalities, confirming the absence of adverse organ-specific effects attributable to the therapy (Supplementary Figs. S8 and S10). These findings affirm the favorable biosafety profile of ATT-CAR-T therapy in vivo, demonstrating its potential as a therapeutic intervention without causing detrimental effects on organ health or triggering systemic inflammation. The comprehensive safety assessment underscores the potential of ATT-CAR-T therapy for clinical translation, providing a solid foundation for its application in treating solid tumors with minimal risk to patient health. This safety assurance, combined with its proven efficacy, positions ATT-CAR-T as a promising candidate for future clinical development and application in cancer immunotherapy.

4. Discussion

Most cancer immunotherapy options depend on the presence of specific tumor biomarkers or antigens [29]. However, these indicators are not always present in all cancer cells, and this challenge may reduce the effectiveness of customized therapy. The current strategies for improving the therapeutic efficacy of CAR-T cells against solid tumor malignancies involve the use of genetically programmed therapeutic T cells to synthesize multidimensional fusion CAR structures [28,30–32]. While these adjunct components of CAR improve CAR-T cell viability and safety on an individual cell basis, they have not demonstrated efficacy improvements for target-negative solid tumors. A primary hurdle in utilizing CAR-T therapy for solid tumors is the limited availability of specific antigens. Crafting CAR-T cells that exclusively target and eliminate tumor cells while sparing healthy tissues poses a significant challenge. Here, we developed ATT-CAR-T cells, which constitute an optimized, peptide-based, target-regulated platform for antigen insertion in target-negative solid tumors; this platform generated one CAR-T-cell to treat multiple tumors and exhibited a significant effect in vivo.

Given the intricate immunological landscape within solid tumors, certain tumor mutations can confer resistance or enable evasion of CAR-T cell-mediated killing. Our previous research has demonstrated that

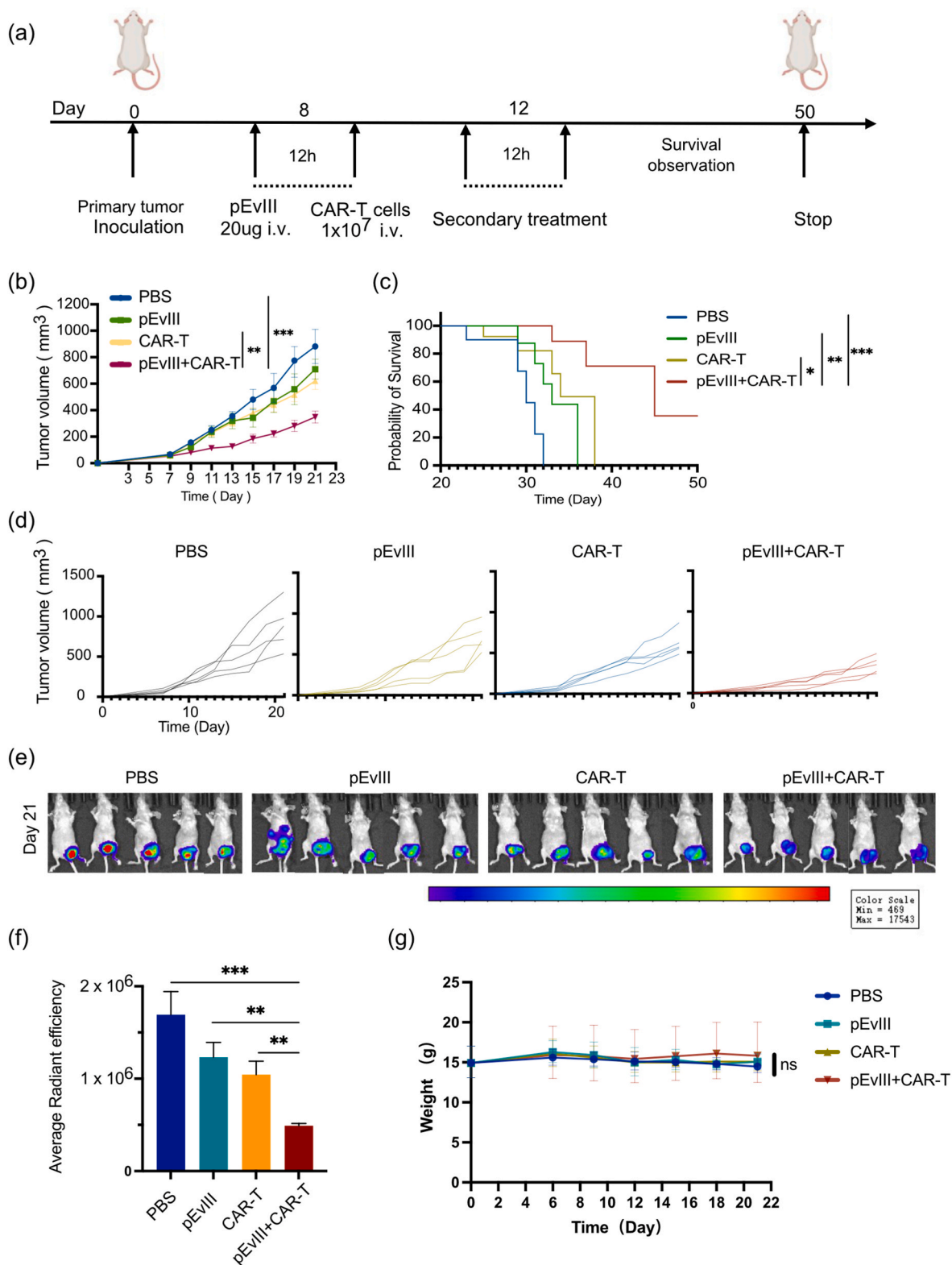


Fig. 5. In vivo antitumor effect of ATT-CAR-T. (a) Schematic illustration of the treatment of ATT-CAR-T in MDA-MB-231-luc model. (b) Tumor growth curves in MDA-MB-231-luc tumor model (n = 5). (c) survival curves in different groups (n = 5). (d) Single tumor volume of each mouse in different groups. (e, f) In vivo bioluminescence images of the MDA-MB-231-luc tumor-bearing mice (n = 5). (g) Weight records of tumor bearing mice that treated with indicated formulation, no obvious weight loss was observed. Data are represented as the mean \pm s.e.m. *P < 0.05, **P < 0.01, ***P < 0.001. A one-way ANOVA was used for statistical analysis (b, e) or log-rank test (c), and a student's t-test was used for statistical analysis(f).

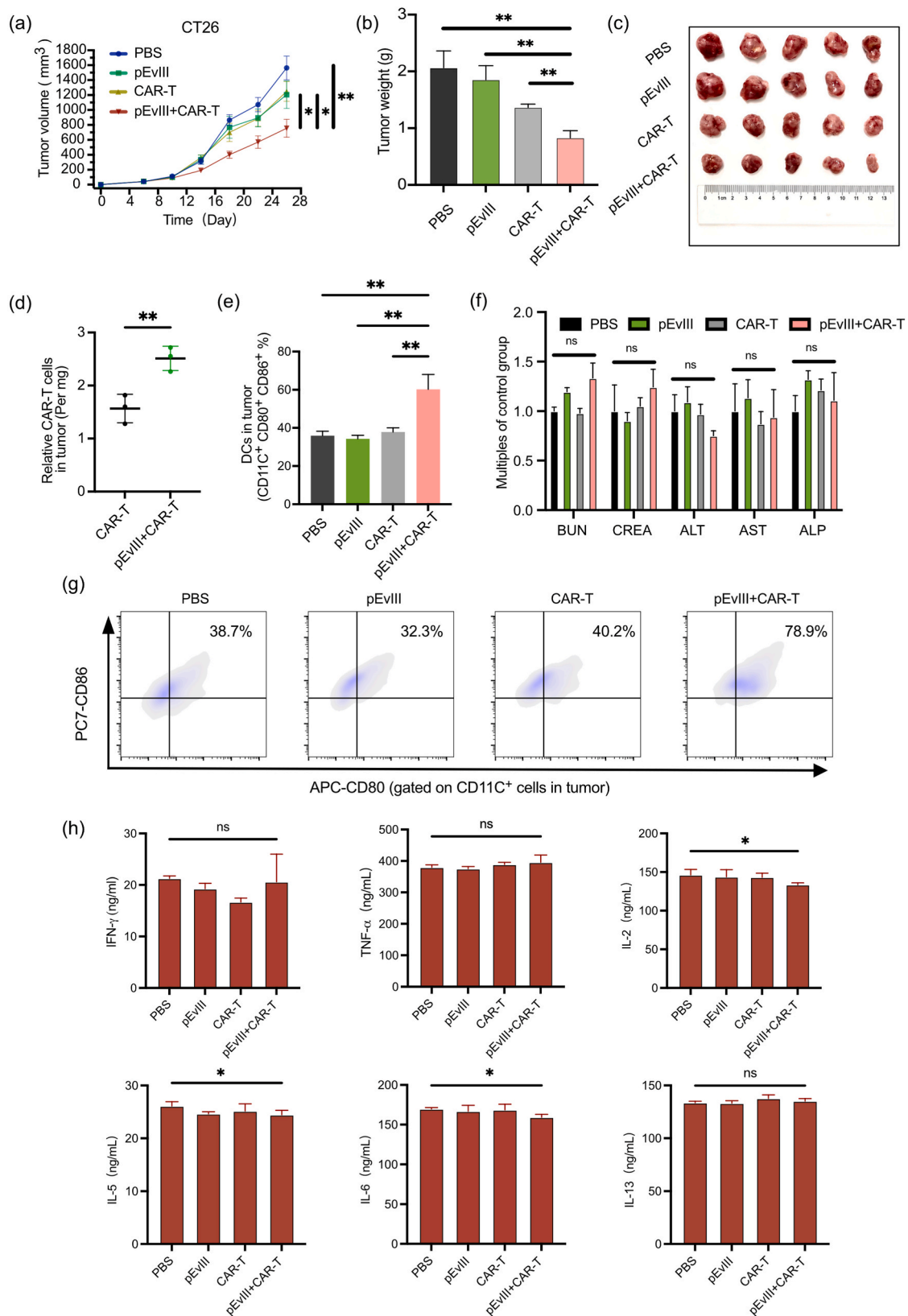


Fig. 6. Evaluation of ATT-CAR-T performance in immunocompetent mouse models.

(a) Tumor growth curves in the CT26 tumor model (n = 5); (b, c) Tumor weight and photographs of tumors harvested from mice in different treatment groups on day 26. (d) Relative levels of CAR-T cells and mature DCs (e) in CT26 tumors of BALB/c mice across different treatment groups on day 26. (f, h) Safety evaluation following immunization with different treatments. Biochemical indexes (BUN, CREA, ALT, AST, ALP) (f) and levels of cytokines (IL-2, IL-5, IL-6, IL-13, TNF- α , and IFN- γ) (h) were measured 48 h after administration. (g) Representative flow cytometry images of DCs in CT26 tumors of BALB/c mice in different treatment groups. Data are presented as the mean \pm s.e.m. *P < 0.05, **P < 0.01. A one-way ANOVA was utilized for statistical analysis (a), while a student's t-test was employed for statistical analysis (b, d, e, f, h).

solid tumors can exploit fusogenic nanoscale systems lacking specific antigens to introduce these antigens and establish TRUE CAR-T therapy [23,33]. Utilizing the fusogenic nanosystem, the corresponding target was efficiently integrated into the tumor cell membrane, eliciting anti-tumor effects while overcoming limitations posed by inherent tumor antigen profiles. In this study, we illustrate how the ATT-CAR-T platform enhances CAR-T cell performance in antigen-lacking solid tumors through antigen modification, underscoring its broad applicability as a leading clinical candidate. However, this represents only an initial exploration of utilizing CAR-T cell therapy for treating solid tumors. We still encounter numerous challenges regarding efficacy, such as addressing potential side effects and ensuring the persistence, expansion, and safety of CAR-T cells [34]. Considering the array of adjuvant therapies currently available in clinical practice, ATT-CAR-T can use these approaches to enhance its clinical efficacy and safety [35,36]. For instance, it can be combined with immune checkpoint inhibitors like PD-1/PD-L1 or radiotherapy to augment the recognition and penetration of CAR-T cells into solid tumors [37,38]. Furthermore, while we employed a second-generation CAR-T design model in this study, more intricate CAR-T designs hold the potential to enhance the efficacy of ATT-CAR-T against solid tumors by improving the persistence and expansion of CAR-T cells. This aspect remains an ongoing endeavor. Additionally, besides being weakly acidic, the tumor microenvironment also exhibits characteristics such as hypoxia [39]. Developing potent targeted delivery carriers tailored to these features can effectively circumvent tumor self-antigen heterogeneity and create opportunities for CAR-T/TCR-T to exert its effects. Strategies involving tumor-specific enzymes or redox reactions also present viable avenues for exploration.

5. Conclusion

In conclusion, we have introduced ATT-CAR-T, a novel and efficient CAR-T therapy strategy that utilizes a peptide, pEvIII, to modify the antigen expression of diverse solid tumor cells. We demonstrated that pEvIII can respond to the acidic environment within tumors without the need for specific antibody-antigen binding. This approach effectively suppresses primary tumor development while maintaining a favorable biosafety profile. Our findings open new avenues for exploring the treatment of solid tumors and position ATT-CAR-T as a promising candidate for clinical application.

CRedit authorship contribution statement

Tianyu Shi: Writing – review & editing, Writing – original draft, Software, Investigation, Formal analysis, Data curation. **Mengna Sun:** Validation, Software, Investigation, Formal analysis, Data curation. **Subiyinuer Tuerhong:** Validation, Supervision, Software, Methodology, Investigation. **Mengru Li:** Software, Resources, Project administration. **Jiayu Wang:** Resources, Methodology. **Yingxin Wang:** Visualization, Validation, Supervision, Software, Resources, Methodology. **Qinghua Zheng:** Visualization, Validation, Supervision. **Lu Zou:** Software, Resources, Methodology. **Changchang Lu:** Validation, Supervision. **Zhichen Sun:** Validation, Supervision. **Zhengyun Zou:** Supervision. **Jie Shao:** Methodology. **Juan Du:** Supervision. **Rutian Li:** Project administration. **Baorui Liu:** Methodology, Investigation. **Fanyan Meng:** Supervision, Project administration, Funding acquisition, Conceptualization.

Declaration of competing interest

The authors declare that they have no known competing financial interests or personal relationships that could have appeared to influence the work reported in this paper.

Data availability

Data will be made available on request.

Acknowledgements

We thank Qiaoli Wang, Aoxing Chen, Xin Zhang, Yi Mei, Xinyu Su for providing PBMC. We thank Xinyu Su for technical support. This work was supported by grants from the National Natural Science Foundation of China (Nos. 82072926, 81930080, 82373280) and Practice Innovation Programs of Jiangsu Province, China (SJCX23_0852).

Appendix A. Supplementary data

Supplementary data to this article can be found online at <https://doi.org/10.1016/j.biomaterials.2024.122607>.

References

- [1] S. Cordoba, S. Onuoha, S. Thomas, D.S. Pignataro, R. Hough, S. Ghorashian, A. Vora, D. Bonney, P. Veys, K. Rao, G. Lucchini, R. Chiesa, J. Chu, L. Clark, M. M. Fung, K. Smith, C. Peticone, M. Al-Hajj, V. Baldan, M. Ferrari, S. Srivastava, R. Jha, F. Arce Vargas, K. Duffy, W. Day, P. Virgo, L. Wheeler, J. Hancock, F. Farzaneh, S. Domning, Y. Zhang, N.Z. Khokhar, V.G.R. Peddareddigari, R. Wynn, M. Pule, P.J. Amrolia, CAR T cells with dual targeting of CD19 and CD22 in pediatric and young adult patients with relapsed or refractory B cell acute lymphoblastic leukemia: a phase 1 trial, *Nat Med* 27 (10) (2021) 1797–1805.
- [2] H. Dai, Z. Wu, H. Jia, C. Tong, Y. Guo, D. Ti, X. Han, Y. Liu, W. Zhang, C. Wang, Y. Zhang, M. Chen, Q. Yang, Y. Wang, W. Han, Bispecific CAR-T cells targeting both CD19 and CD22 for therapy of adults with relapsed or refractory B cell acute lymphoblastic leukemia, *J. Hematol. Oncol.* 13 (1) (2020) 30.
- [3] Y. Hu, Y. Zhou, M. Zhang, W. Ge, Y. Li, L. Yang, G. Wei, L. Han, H. Wang, S. Yu, Y. Chen, Y. Wang, X. He, X. Zhang, M. Gao, J. Yang, X. Li, J. Ren, H. Huang, CRISPR/Cas9-Engineered universal CD19/CD22 dual-targeted CAR-T cell therapy for relapsed/refractory B-cell acute lymphoblastic leukemia, *Clin. Cancer Res.* 27 (10) (2021) 2764–2772.
- [4] N. Pang, J. Shi, L. Qin, A. Chen, Y. Tang, H. Yang, Y. Huang, Q. Wu, X. Li, B. He, T. Li, B. Liang, J. Zhang, B. Cao, M. Liu, Y. Feng, X. Ye, X. Chen, L. Wang, Y. Tian, H. Li, J. Li, H. Hu, J. He, Y. Hu, C. Zhi, Z. Tang, Y. Gong, F. Xu, L. Xu, W. Fan, M. Zhao, D. Chen, H. Lian, L. Yang, P. Li, Z. Zhang, IL-7 and CCL19-secreting CAR-T cell therapy for tumors with positive glypican-3 or mesothelin, *J. Hematol. Oncol.* 14 (1) (2021) 118.
- [5] C. Qi, J. Gong, J. Li, D. Liu, Y. Qin, S. Ge, M. Zhang, Z. Peng, J. Zhou, Y. Cao, X. Zhang, Z. Lu, M. Lu, J. Yuan, Z. Wang, Y. Wang, X. Peng, H. Gao, Z. Liu, H. Wang, D. Yuan, J. Xiao, H. Ma, W. Wang, Z. Li, L. Shen, Claudin18.2-specific CAR T cells in gastrointestinal cancers: phase 1 trial interim results, *Nat Med* 28 (6) (2022) 1189–1198.
- [6] R. Huang, X. Li, Y. He, W. Zhu, L. Gao, Y. Liu, L. Gao, Q. Wen, J.F. Zhong, C. Zhang, X. Zhang, Recent advances in CAR-T cell engineering, *J. Hematol. Oncol.* 13 (1) (2020) 86.
- [7] R.C. Sterner, R.M. Sterner, CAR-T cell therapy: current limitations and potential strategies, *Blood Cancer J.* 11 (4) (2021) 69.
- [8] S. Ma, X. Li, X. Wang, L. Cheng, Z. Li, C. Zhang, Z. Ye, Q. Qian, Current progress in CAR-T cell therapy for solid tumors, *Int. J. Biol. Sci.* 15 (12) (2019) 2548–2560.
- [9] E. Boedtker, L. Bunch, S.F. Pedersen, Physiology, pharmacology and pathophysiology of the pH regulatory transport proteins NHE1 and NBCn1: similarities, differences, and implications for cancer therapy, *Curr Pharm Des* 18 (10) (2012) 1345–1371.
- [10] E. Boedtker, S.F. Pedersen, The acidic tumor microenvironment as a Driver of cancer, *Annu. Rev. Physiol.* 82 (2020) 103–126.
- [11] J.F. Hunt, P. Rath, K.J. Rothschild, D.M. Engelman, Spontaneous, pH-dependent membrane insertion of a transbilayer alpha-helix, *Biochemistry* 36 (49) (1997) 15177–15192.
- [12] L.C. Wyatt, J.S. Lewis, O.A. Andreev, Y.K. Reshetnyak, D.M. Engelman, Applications of pHILIP technology for cancer imaging and therapy, *Trends Biotechnol.* 35 (7) (2017) 653–664.
- [13] M.P. Antosh, D.D. Wijesinghe, S. Shrestha, R. Lanou, Y.H. Huang, T. Hasselbacher, D. Fox, N. Neretti, S. Sun, N. Katenka, L.N. Cooper, O.A. Andreev, Y.K. Reshetnyak, Enhancement of radiation effect on cancer cells by gold-pHILIP, *Proc Natl Acad Sci U S A* 112 (17) (2015) 5372–5376.
- [14] L. Yao, J. Daniels, A. Moshnikova, S. Kuznetsov, A. Ahmed, D.M. Engelman, Y. K. Reshetnyak, O.A. Andreev, pHILIP peptide targets nanogold particles to tumors, *Proc Natl Acad Sci U S A* 110 (2) (2013) 465–470.
- [15] X. Zhang, N. Rotllan, A. Canfran-Duque, J. Sun, J. Toczek, A. Moshnikova, S. Malik, N.L. Price, E. Araldi, W. Zhong, M.M. Sadeghi, O.A. Andreev, R. Bahal, Y. K. Reshetnyak, Y. Suarez, C. Fernandez-Hernando, Targeted suppression of miRNA-33 using pHILIP improves Atherosclerosis regression, *Circ. Res.* 131 (1) (2022) 77–90.
- [16] H.K. Gan, A.N. Cvrljevic, T.G. Johns, The epidermal growth factor receptor variant III (EGFRvIII): where wild things are altered, *FEBS J.* 280 (21) (2013) 5350–5370.

- [17] R. Iurlaro, I. Waldhauer, E. Planas-Rigol, E. Bonfill-Teixidor, A. Arias, V. Nicolini, A. Freimoser-Grundschober, I. Cuartas, A. Martinez-Moreno, F. Martinez-Ricarte, E. Cordero, M. Cicuendez, S. Casalino, X. Guardia-Reyes, L. Fahrni, T. Poschinger, V. Steinhart, M. Richard, S. Briner, J. Mueller, F. Osl, J. Sam, S. Colombetti, M. Bacac, C. Klein, E. Pineda, L. Reyes-Figueroa, A. Di Somma, J. Gonzalez, P. Nuciforo, J. Carles, M. Vieito, J. Tabernero, P. Umana, J. Seoane, A novel EGFRvIII T-cell bispecific antibody for the treatment of glioblastoma, *Mol Cancer Ther* 21 (10) (2022) 1499–1509.
- [18] P. Li, L. Yang, T. Li, S. Bin, B. Sun, Y. Huang, K. Yang, D. Shan, H. Gu, H. Li, The Third generation anti-HER2 chimeric antigen receptor mouse T cells alone or together with anti-PD1 antibody inhibits the growth of mouse breast tumor cells expressing HER2 in vitro and in immune competent mice, *Front. Oncol.* 10 (2020) 1143.
- [19] D. Espie, E. Donnadieu, New insights into CAR T cell-mediated killing of tumor cells, *Front. Immunol.* 13 (2022) 1016208.
- [20] R.C. Larson, M.C. Kann, S.R. Bailey, N.J. Haradhvala, P.M. Llopis, A.A. Bouffard, I. Scarfo, M.B. Leick, K. Grauwet, T.R. Berger, K. Stewart, P.V. Anekal, M. Jan, J. Joung, A. Schmidts, T. Ouspenskaia, T. Law, A. Regev, G. Getz, M.V. Maus, CAR T cell killing requires the IFN γ pathway in solid but not liquid tumours, *Nature* 604 (7906) (2022) 563–570.
- [21] T. Morisaki, D.H. Yuzuki, R.T. Lin, L.J. Foshag, D.L. Morton, D.S. Hoon, Interleukin 4 receptor expression and growth inhibition of gastric carcinoma cells by interleukin 4, *Cancer Res.* 52 (21) (1992) 6059–6065.
- [22] X. Song, B. Traub, J. Shi, M. Kornmann, Possible roles of interleukin-4 and -13 and their receptors in gastric and colon cancer, *Int. J. Mol. Sci.* 22 (2) (2021).
- [23] Z. Sun, R. Li, Y. Shen, S. Tan, N. Ding, R. Xu, X. Wang, J. Wei, B. Liu, F. Meng, In situ antigen modification-based target-redirected universal chimeric antigen receptor T (TRUE CAR-T) cell therapy in solid tumors, *J. Hematol. Oncol.* 15 (1) (2022) 29.
- [24] K. Hildner, B.T. Edelson, W.E. Purtha, M. Diamond, H. Matsushita, M. Kohyama, B. Calderon, B.U. Schraml, E.R. Unanue, M.S. Diamond, R.D. Schreiber, T. L. Murphy, K.M. Murphy, Batf3 deficiency reveals a critical role for CD8 α + dendritic cells in cytotoxic T cell immunity, *Science* 322 (5904) (2008) 1097–1100.
- [25] S. Badrinath, M.O. Dellacherie, A. Li, S. Zheng, X. Zhang, M. Sobral, J.W. Pyrdol, K. L. Smith, Y. Lu, S. Haag, H. Ijaz, F. Connor-Stroud, T. Kaisho, G. Dranoff, G. C. Yuan, D.J. Mooney, K.W. Wucherpfennig, A vaccine targeting resistant tumours by dual T cell plus NK cell attack, *Nature* 606 (7916) (2022) 992–998.
- [26] O.S. Blomberg, L. Spagnuolo, H. Garner, L. Voorwerk, O.I. Isaeva, E. van Dyk, N. Bakker, M. Chalabi, C. Klaver, M. Duijst, K. Kersten, M. Bruggemann, D. Pastoors, C.S. Hau, K. Vrijland, E.A.M. Raeven, D. Kaldenbach, K. Kos, I. S. Afonina, P. Kaptein, L. Hoes, W. Theelen, P. Baas, E.E. Voest, R. Beyaert, D. S. Thommen, L.F.A. Wessels, K.E. de Visser, M. Kok, IL-5-producing CD4(+) T cells and eosinophils cooperate to enhance response to immune checkpoint blockade in breast cancer, *Cancer Cell* 41 (1) (2023) 106–123 e10.
- [27] X. Yao, J. Huang, H. Zhong, N. Shen, R. Faggioni, M. Fung, Y. Yao, Targeting interleukin-6 in inflammatory autoimmune diseases and cancers, *Pharmacol. Ther.* 141 (2) (2014) 125–139.
- [28] Q. Zhang, M.E. Hresko, L.K. Picton, L. Su, M.J. Hollander, S. Nunez-Cruz, Z. Zhang, C.A. Assenmacher, J.T. Sockolosky, K.C. Garcia, M.C. Milone, A human orthogonal IL-2 and IL-2R β system enhances CAR T cell expansion and antitumor activity in a murine model of leukemia, *Sci. Transl. Med.* 13 (625) (2021) eabg6986.
- [29] M. Russano, A. Napolitano, G. Ribelli, M. Iuliani, S. Simonetti, F. Citarella, F. Pantano, E. Dell'Aquila, C. Anesi, N. Silvestris, A. Argentiero, A.G. Solimando, B. Vincenzi, G. Tonini, D. Santini, Liquid biopsy and tumor heterogeneity in metastatic solid tumors: the potentiality of blood samples, *J. Exp. Clin. Cancer Res.* 39 (1) (2020) 95.
- [30] A. Hyrenius-Wittsten, Y. Su, M. Park, J.M. Garcia, J. Alavi, N. Perry, G. Montgomery, B. Liu, K.T. Roybal, SynNotch CAR circuits enhance solid tumor recognition and promote persistent antitumor activity in mouse models, *Sci. Transl. Med.* 13 (591) (2021).
- [31] S. Rafiq, O.O. Yeku, H.J. Jackson, T.J. Purdon, D.G. van Leeuwen, D.J. Drakes, M. Song, M.M. Miele, Z. Li, P. Wang, S. Yan, J. Xiang, X. Ma, V.E. Seshan, R. C. Hendrickson, C. Liu, R.J. Brentjens, Targeted delivery of a PD-1-blocking scFv by CAR-T cells enhances anti-tumor efficacy in vivo, *Nat. Biotechnol.* 36 (9) (2018) 847–856.
- [32] J.H. Choe, P.B. Watchmaker, M.S. Simic, R.D. Gilbert, A.W. Li, N.A. Krasnow, K. M. Downey, W. Yu, D.A. Carrera, A. Celli, J. Cho, J.D. Briones, J.M. Duecker, Y. E. Goretsky, R. Dannenfels, L. Cardarelli, O. Troyanskaya, S.S. Sidhu, K. T. Roybal, H. Okada, W.A. Lim, SynNotch-CAR T cells overcome challenges of specificity, heterogeneity, and persistence in treating glioblastoma, *Sci. Transl. Med.* 13 (591) (2021).
- [33] R. Xu, Q. Wang, J. Zhu, Y. Bei, Y. Chu, Z. Sun, S. Du, S. Zhou, N. Ding, F. Meng, B. Liu, Membrane fusogenic nanoparticle-based HLA-peptide-addressing universal T cell receptor-engineered T (HAUL TCR-T) cell therapy in solid tumor, *Bioengineering & Translational Medicine* 8 (6) (2023) e10585.
- [34] M.L. Schubert, M. Schmitt, L. Wang, C.A. Ramos, K. Jordan, C. Muller-Tidow, P. Dreger, Side-effect management of chimeric antigen receptor (CAR) T-cell therapy, *Ann. Oncol.* 32 (1) (2021) 34–48.
- [35] S. Srivastava, S.N. Furlan, C.A. Jaeger-Ruckstuhl, M. Sarvothama, C. Berger, K. S. Smythe, S.M. Garrison, J.M. Specht, S.M. Lee, R.A. Amezcua, V. Voillet, V. Muhunthan, S. Yechan-Gunja, S.P.S. Pillai, C. Rader, A.M. Houghton, R. H. Pierce, R. Gottardo, D.G. Maloney, S.R. Riddell, Immunogenic chemotherapy enhances recruitment of CAR-T cells to lung tumors and improves antitumor efficacy when combined with checkpoint blockade, *Cancer Cell* 39 (2) (2021) 193–208 e10.
- [36] V.M. Qin, N.M. Haynes, C. D'Souza, P.J. Neeson, J.J. Zhu, CAR-T plus radiotherapy: a promising combination for immunosuppressive tumors, *Front. Immunol.* 12 (2021) 813832.
- [37] R. Grosser, L. Cherkassky, N. Chintala, P.S. Adusumilli, Combination immunotherapy with CAR T cells and checkpoint blockade for the treatment of solid tumors, *Cancer Cell* 36 (5) (2019) 471–482.
- [38] I. Minn, S.P. Rowe, M.G. Pomper, Enhancing CAR T-cell therapy through cellular imaging and radiotherapy, *Lancet Oncol.* 20 (8) (2019) e443–e451.
- [39] X. Wei, Y. Chen, X. Jiang, M. Peng, Y. Liu, Y. Mo, D. Ren, Y. Hua, B. Yu, Y. Zhou, Q. Liao, H. Wang, B. Xiang, M. Zhou, X. Li, G. Li, Y. Li, W. Xiong, Z. Zeng, Mechanisms of vasculogenic mimicry in hypoxic tumor microenvironments, *Mol. Cancer* 20 (1) (2021) 7.